



OPEN

Effect of ultrasonication on the stability and storage of a soy protein isolate-phosphatidylcholine nanoemulsions

Fei Teng^{1,4}, Mingyu He^{1,4}, Jingwen Xu¹, Fanfan Chen¹, Changling Wu¹, Zhongjiang Wang¹ & Yang Li^{1,2,3}✉

Phosphatidylcholine-soybean protein isolate (PC-SPI) nanoemulsions were prepared by ultrasonication. The effects of preparation conditions (SPI and PC addition, ultrasonic power and time) on the structural properties of the nanoemulsions and their storage stability were investigated. The results showed that the most optimal adsorption capacity and adsorption tightness at the oil–water interface under optimal conditions (1.5% SPI, 0.20% PC, 500 W ultrasonic power and 9 min ultrasonic time) were exhibited by the SPI-PC conjugate, which demonstrated that this nanoemulsions can be categorized as a high-quality emulsion suitable for research. To test its stability, and the high-quality nanoemulsion of β -carotene was stored. After degradation of the nanoemulsions during storage, β -carotene was released. The β -carotene retention rate of the high-quality emulsion was maintained above 86% at different temperatures in the absence of light for up to 30 days. This study provides new information for the development of transport and stability systems for nanoemulsions.

Nanoemulsions are carriers with strong kinetic stability and bioavailability that are used to transport lipophilic substances¹. Compared with conventional emulsions, nanoemulsions with particle sizes of mainly 100–500 nm have higher stability, solubility, bioavailability, and transport efficiency². Nanoemulsions can increase the availability of biologically active substances in specific parts via controlled release³. Nanoemulsions are usually prepared using a high-energy (mechanically based) or low-energy (chemically based) method. High energy technologies such as homogenization, microfluidization and ultrasound technology have been used to prepare nanoemulsions⁴. However, microfluidic and homogenization technologies were not readily available in industry due to high costs and scalability issues⁵. Ultrasonic processing has the advantages of easy operation of the system, low production cost, low requirements for instruments and high energy efficiency⁶. Hydraulic shear and cavitation are produced by ultrasonication to break droplets to nanodroplets^{7,8}.

Soybean protein isolate (SPI) is widely used in food formulations due to its nutritional value and functional characteristics⁹. SPI as an emulsifier plays a vital role in the formation of small oil droplets. The introduction of external emulsifiers (such as lecithin) can enhance the emulsification properties of SPI in producing nanoemulsions¹⁰. Phosphatidylcholine (PC) is the main phospholipid in lecithin¹¹. Lecithin contains a lipophilic group in the form of a fatty acid group and a hydrophilic group in the form of a phosphate. The amphiphilic molecular structure is responsible for the excellent emulsification ability of PC, and the physical stability of an SPI nanoemulsion can be increased by adding lecithin^{12,13}. Emulsifiability increases when PC interacts with SPI through a hydrophobic group. Li et al.¹⁴ proved that a binding site can be a hydrophobic region of the α -helix of a protein.

β -Carotene (C₄₀H₅₆) is a natural pigment that is found in various fruits, grains, and oils. It is a lipophilic substance and a highly conjugated long-chain isoprenoid micronutrient¹⁵. β -Carotene has been widely used in food, feed, and other nutraceuticals as an antioxidant¹⁶. Some functionalities of β -carotene are limited because its lower chemical stability of carotenoids, which is easily degraded by heat, oxygen, and light. Because the solubility

¹College of Food Science, Northeast Agricultural University, Harbin 150030, Heilongjiang, China. ²Harbin Institute of Food Industry, Harbin 150030, Heilongjiang, China. ³Heilongjiang Academy of Green Food Science, Harbin 150030, Heilongjiang, China. ⁴These authors contributed equally: Fei Teng and Mingyu He. ✉email: yangli@neau.edu.cn

of β -carotene in some common solvents, such as water, dimethyl sulfoxide (DMSO), and ethanol, is very low, it is difficult to add it to foods to maintain its stability¹⁷. β -Carotene can be dissolved in oil at 25 °C, and the bioavailability of β -carotene can be increased by combining it with digestible lipids in the human body¹⁶. In addition, the biological activity of β -carotene against heart disease, cataracts, and cancer has been previously demonstrated¹⁸. Therefore, the emergence of nanoemulsions provide a new way for the successful transportation of β -carotene.

Emulsification, aggregation, flocculation, and precipitation may occur in emulsions due to unstable thermodynamic systems¹⁹. Nanoemulsions that are physicochemically stable can provide some ζ -potential advantages that can be used in the development of food. Temperature, pH, storage time, processing method, and ionic strength influence the stability of emulsions²⁰. The main factors affecting emulsion stability were temperature and time during storage. In this research, ultrasound was used to prepare soybean protein-phosphatidylcholine nanoemulsion, and β -carotene was embedded into nanoemulsion to improve the stability and bioavailability of β -carotene. After preparing the nanoemulsion, the best preparation process of β -carotene nanoemulsion was determined. In addition, their stability was checked, and the effect of different storage temperature and storage time on the stability of the nanoemulsion was determined to ensure β -carotene. The stability of nanoemulsion during storage and transportation to expand its application in food processing.

Materials and methods

Materials. SPI and PC (Liao Cheng, Shandong, China) were obtained from Gao Tang Co. Ltd., and sunflower oil (Duoli Group Co., Ltd., Shanghai, China) was obtained from a local supermarket. β -Carotene ($\geq 97.0\%$) and acetone (insoluble content $> 95\%$) were purchased from Sigma-Aldrich (St. Louis, MO, USA). Other compounds (analytical reagent grade) were obtained from the Kemiou Chemical Reagent Co., Ltd (Tianjing, China).

β -Carotene nanoemulsion preparation. SPI (0.5%, 1.0%, 1.5%, 2.0%, 2.5%, 3.0%) was mixed with PC (0.13%, 0.15%, 0.17%, 0.19%, 0.21%, 0.23%) with varying ratios before being dispersed in phosphate buffer solution (10.0 mM phosphate buffer, pH 7.5, 0.01% (w/w) sodium azide) followed by mixing at room temperature (25 °C) for 30 min using magnetic stirring¹¹. β -Carotene ($\geq 97.0\%$, 0.01 g, w/w) and sunflower oil (5 g, w/w) were mixed and magnetically stirred at room temperature for 30 min under the same conditions. The water and oil phase were homogenized with an Ultra-Turrax T18 homogenizer (Angni Co. Ltd., Shanghai, China) at room temperature at 20,000 rpm for 5 min to form a coarse emulsion. Ultrasonic treatment used a titanium probe with a diameter of 0.636 cm for ultrasonic cell disruption (Washin Instrument Co. Ltd., Wuxi, Jiangsu, China). The coarse emulsion was poured into a beaker surrounded by a double-walled cooling water jacket to minimize increases in temperature. Ultrasonic treatment at a frequency of 20 kHz and various output powers (200, 300, 400, 500 or 600 W), various treatment times (6, 7, 8, 9 or 10 min), pulse duration 4 s, off time 2 s. The freshly-prepared (O/W) emulsion was used for the following studies.

Particle size, ζ -potential, and polydispersity index (PDI) analysis. The particle size, ζ -potential and PDI of nanoemulsions were measured using a dynamic light-scattering device (Zetasizer Nano-ZS 90 light scattering particle size analyzer). Nanoemulsions were diluted (1:1,000) with a phosphate buffer before measurement to prevent multiple scattering²¹. Aqueous dispersion and the refractive index medium were set at 1.33 and 1.45, respectively. The fresh nanoemulsions and phosphate buffer were diluted in proportion (1:100, v/v) during ζ -potential analysis.

Turbidity analysis. Turbidity values were obtained using a previously published method with slight modification²². The nanoemulsions were diluted 40 times with a phosphate buffer solution. The absorbance was measured at 600 nm with a spectrophotometer (LW-1600FC UV, Shanghai, China). Phosphate buffer solution was used as a blank. Turbidity was calculated using the formula:

$$T = 2.302 \times \frac{A \times V}{I} \quad (1)$$

where A = the absorbance of diluted nanoemulsions at 600 nm, I = optical path extent (0.01 m), and V = dilution (40).

Emulsification yield analysis. The emulsification yield of the nanoemulsions was determined using a previously published method¹¹. The β -carotene in 1 mL of the nanoemulsions was extracted using an organic phase (ethanol: n-hexane = 1:1, 95%, 5 mL) and was quantitated using an Agilent 1,100 HPLC (Agilent Technologies Inc., Santa Clara, CA, USA) system with a UV-Vis diode array absorption detector. A reversed phase analytical column C30 (YMC Carotenoid, 250 \times 4.6 mm i.d., 5 μ m, YMC, Inc., Wilmington, NC, USA) was used with a flow rate of 1.0 mL/min by mobile phase. A 20- μ L sample was analyzed using a diode array detector (DAD) at 450 nm. Standard curves were obtained using different concentrations of β -carotene standard samples (assuming a purity of 100%). The amount of β -carotene in the nanoemulsions was determined after processing the data with Dionex Chromeleon software. The emulsion yield (%) of the nanoemulsions was calculated by the following formula:

$$\text{Emulsification yield} = \frac{\beta - \text{carotene content in nanoemulsion}}{\text{total } \beta - \text{carotene content}} \times 100 \quad (2)$$

SPI addition	Particle size (nm)	ζ-potential (mV)	PDI	Emulsification yield (%)	Turbidity	TSI
0.5	797.0 ± 7.8 ^a	-28.90 ± 0.27 ^d	0.56 ± 0.01 ^b	69.11 ± 0.62 ^f	26,758.4 ± 256.7 ^a	5.50 ± 0.05 ^a
1.0	606.0 ± 5.9 ^b	-29.50 ± 0.28 ^c	0.44 ± 0.01 ^d	78.20 ± 0.71 ^c	21,150.8 ± 201.1 ^b	4.30 ± 0.04 ^b
1.5	295.6 ± 2.8 ^f	-33.40 ± 0.32 ^a	0.21 ± 0.01 ^f	90.03 ± 0.83 ^a	14,896.6 ± 139.9 ^e	3.21 ± 0.03 ^c
2.0	382.3 ± 5.6 ^e	-33.30 ± 0.32 ^a	0.37 ± 0.01 ^e	81.25 ± 0.74 ^b	18,561.0 ± 175.5 ^d	3.41 ± 0.03 ^d
2.5	471.5 ± 4.6 ^d	-30.50 ± 0.29 ^b	0.52 ± 0.01 ^c	76.48 ± 0.69 ^d	19,420.3 ± 1836.4 ^{bc}	3.90 ± 0.04 ^c
3.0	549.0 ± 5.5 ^c	-29.60 ± 0.28 ^c	0.66 ± 0.01 ^a	70.02 ± 0.63 ^e	20,837.7 ± 198.8 ^b	4.21 ± 0.04 ^b

Table 1. Effect of the soybean protein content on the characteristics and stability of nanoemulsions. Data represent mean ± standard deviations. Different letters in the same column represent a significant difference between samples ($p < 0.05$). Arrange all the averages in descending order, and use the letter “a” on the maximum average.

Nanoemulsion stability analysis. Nanoemulsion stability was determined with a Turbiscan optical scanning analyzer (France Formulaction Company, Toulouse, France) according on the variation in the backscattering light intensity at different locations of the test tube using a previously published method with slight modification²³. The analyzer was equipped with two detectors and a pulsed near-infrared light source ($\lambda = 880$ nm). The measurement process mainly used the central portion of the reflected spot, whereby the particle volume concentration and average particle size were directly related to the measured reflected light. Next, 20 mL of different loadings of β -carotene samples was placed in a cylindrical glass cell and then analyzed in the Turbiscan with scanning (from the bottom to the top) every 30 min for 6 h at 30 °C. The dynamic change in the reflected amount of light (ΔBS) indicated the stability of the SPI-PC nanoemulsions. The Turbiscan Stability Index (TSI) was calculated using the formula:

$$TSI = \sqrt{\frac{\sum_{i=1}^n (x_i - x_{BS})^2}{n - 1}} \quad (3)$$

where x_i = the average scattering intensity per minute, x_{BS} = the average value of x_i , and n = the number of scans.

Raman microscopic observation of nanoemulsion morphology. Raman microscopic observation was used as an interface structural analysis of the nanoemulsions²⁰. A 5 mW laser was focused on a slide with droplets in the center, and the droplets were observed. The scanning distance was set in the direction of the two axes (x-axis, y-axis) according to the required scanning range. Spectral analysis was performed using Spec 32 software, which was supplied with the spectrometer. The moving distance of the spot was 2 μ m, which enabled automatic and efficient scanning of the nanoemulsion sample to be tested. The 3D imaging portion observed by the microscope was based on 2D imaging. The laser focusing depth (i.e., z-axis) was adjusted so that layer-by-layer scanning of the sample could be manually conducted.

Nanoemulsion storage stability. The β -carotene nanoemulsions were prepared with 1.5% SPI, 0.17% PC, ultrasonic power 500 W, and ultrasonic time 9 min. The storage stability of the β -carotene nanoemulsions was evaluated by adding 1 mL of the emulsion to a brown tube (1.5 mL) that was stored at 4, 25, or 55 °C²⁴. Next, 1 mL sample was extracted with 5 mL of n-hexane: ethanol = 3:2, and the hexane phase was removed. After repeating twice, their absorbances were measured using a spectrophotometer at 450 nm. A standard curve of β -carotene was prepared under similar conditions, and the β -carotene concentration was measured. The β -carotene retention rate was calculated using the formula:

$$R_{\beta\text{-carotene}} = \frac{C_N}{C_I} \times 100\% \quad (4)$$

where $R_{\beta\text{-carotene}}$ denotes β -carotene retention, C_N indicates the concentration of β -carotene in the nanoemulsions, and C_I represents the initial concentration of β -carotene.

Statistical analysis. All measurements were analyzed by t-test via SPSS 16 software, and the results are expressed as the mean ± standard deviation (SD). Analysis of variance (ANOVA) was used to determine differences between groups.

Results

Effect of SPI addition. The effect of SPI addition on the characteristics and stability of nanoemulsions is shown in Table 1. The average particle size, PDI, turbidity, and TSI of the nanoemulsions were drastically decreased with the SPI content increased from 0.5% to 1.5%. The particle size value, turbidity, TSI and PDI value were minimized when the SPI addition was 1.5%. Hebishi found that when the whey protein content was low, the prepared nanoemulsions had larger droplets, which was consistent with the current results²⁵. SPI as an emulsifier plays a vital role in the formation of small oil droplets by reducing the tension at the oil–water interface. When SPI is adsorbed on the surface of oil droplets, it prevents the oil droplets from accumulating and coalescing²⁶. The thickness of the interfacial layer gradually increased and the interfacial tension at the oil–water

PC addition	Particle size (nm)	ζ -potential (mV)	PDI	Emulsification yield (%)	Turbidity	TSI
0.13	604.5 ± 5.6 ^a	-26.90 ± 0.26 ^f	0.73 ± 0.01 ^a	88.11 ± 0.83 ^c	26,311.0 ± 253.0 ^a	5.00 ± 0.04 ^a
0.15	470.2 ± 4.1 ^c	-28.20 ± 0.27 ^e	0.60 ± 0.01 ^b	88.90 ± 0.84 ^b	23,986.8 ± 229.0 ^d	3.91 ± 0.03 ^b
0.17	295.6 ± 2.6 ^f	-33.40 ± 0.32 ^{ab}	0.21 ± 0.01 ^c	90.03 ± 0.83 ^a	22,670.4 ± 216.4 ^e	3.10 ± 0.02 ^c
0.19	332.3 ± 3.0 ^e	-33.70 ± 0.32 ^a	0.41 ± 0.01 ^d	90.15 ± 0.84 ^a	24,732.7 ± 234.1 ^c	3.20 ± 0.02 ^d
0.21	401.5 ± 3.7 ^d	-32.10 ± 0.31 ^c	0.53 ± 0.01 ^c	84.20 ± 0.79 ^d	25,082.6 ± 235.9 ^b	3.40 ± 0.02 ^c
0.23	483.1 ± 4.3 ^b	-31.40 ± 0.30 ^d	0.64 ± 0.01 ^b	78.13 ± 0.73 ^e	26,439.8 ± 253.0 ^a	4.00 ± 0.03 ^b

Table 2. Effect of the lecithin content on the characteristics and stability of nanoemulsions. Data represent mean ± standard deviations. Different letters in the same column represent a significant difference between samples ($p < 0.05$). Arrange all the averages in descending order, and use the letter “a” on the maximum average.

interface decreased with SPI concentration, which increased the stability of the emulsion. High interfacial tension caused the emulsion droplets to fuse and aggregate with each other²⁷. The maximum concentration of SPI adsorbed at the interface is the critical micelle concentration. If the amount of SPI adsorption at the interface exceeded a critical value, the adsorption capacity of the protein molecule was weakened at the interface of the continuous phase.

The stability of the nanoemulsion was positively correlated with its ζ -potential¹¹. Table 1 showed that the absolute value of the ζ -potential was greater than 30 mV between 1.5% SPI and 2.5% SPI. It was observed that the ζ -potential values had a maximal value (-33.4 mV) at 1.5% SPI. The nanoemulsions exhibited satisfactory stability through electrostatic repulsion above 30 mV of the ζ -potential value²⁸. It could be deduced that the nanoemulsions stabilized by SPI-PC complex had a high stability. With increasing addition of protein, the unadsorbed soluble protein formed aggregates under the action of ultrasonic cavitation and thermal effects due to enhanced hydrophobic interactions²⁰. The protein at the oil–water interface was replaced by aggregates, leading to a decrease in emulsion stability²⁹. Ghosh⁵ found that water molecules were difficult to penetrate the protein molecules under highly protein concentration. Protein molecules were aggregated, which decreased the stability of the nanoemulsions. Therefore, the emulsion yield value and the TSI value of the nanoemulsions were reduced.

Effect of PC addition. PC is a surfactant with excellent biocompatibility and amphiphilicity, and it can increase the load capacity and reduce the interfacial tension of the dispersed phase by forming an embedded structure at the water/oil interface³⁰. PC interacts with soy protein through electrostatic and hydrophobic interactions, and significantly affects the functional properties of soy protein³¹. The hydrophobic region of SPI can bind to the hydrophobic group of PC, and the binding force will maintain the interaction between SPI and PC^{14,32}. Thus, The particle size, PDI value, TSI and turbidity of SPI-PC nanoemulsions were increased with the addition of PC from 0.13% to 0.17% as shown in Table 2. The smaller droplets were formed when the PC was increased due to sufficient protein isolate and insufficient interfacial tension to maintain newly formed droplets⁷ and thus, the stability of SPI-PC nanoemulsion was enhanced by adding more PC. This mixture system lowered the interfacial tension and also prevented coalescence, and thus improved the stability of a protein-stabilized oil–water emulsion³³. Moreover, the soy protein molecule was negatively charged at neutral pH, while PC was a zwitterion with both positive and negative charges³⁴. The addition of PC could increase the interface adsorption by enhancing the electrostatic interaction between hydrophobic SPI and PC. In the case of the emulsification interface, the blank palce found in soy protein was subsequently filled with PC.

This mixture system lowers the interfacial tension and also prevents coalescence, and thus improves the stability of a protein-stabilized oil–water emulsion³³. Therefore, after PC addition (from 0.13 to 0.19%), the ζ -potential value and the stability of the nanoemulsions were increased. Excessive PC addition increased the PC content in the aqueous phase of the emulsion. Based on the principle of displacement solubilisation, the oil–water interface protein was replaced by PC and entered the aqueous phase, which reduced the interfacial protein content and increased the particle size of the emulsion^{35–37}.

Effect of ultrasonic power. Ultrasonication is more economical and practical than microfluidization when taking into consideration production costs, maintenance, and aseptic production. Ultrasonication has become an excellent and superior tool in the emulsification process³⁸. As shown in Table 3, an increase in ultrasonic power (from 100 to 400 W) led to an increase in average particle size, PDI, and TSI, but a decrease in turbidity value, which in turn increased ζ -potential and emulsion production. The cavitation effect produced by ultrasonication can reduce the particle size of SPI and affect the interfacial layer of the emulsion³⁹. As ultrasonic power increased, the distribution became more uniform. These results suggest that 500 W resulted in the best values. After the ultrasonic power is increased to 500 W, the formation and collapse of cavitation bubbles can generate strong shock waves and jets. This strong force causes a significant increase in particle size and PDI that results in the tendency of the emulsion to re-agglomerate. Research has shown that the hydrophobicity of milk proteins was reported to have increased after ultrasonication^{40,41}. The hydrophobic interaction forces aggregated droplets and increased the PDI, turbidity, and particle size of the emulsion. The increase in the of ultrasonic power increased the frequency of collisions between emulsion droplets, which subsequently leads to a higher probability of coalescence of droplets²⁸. The increasing turbidity values may be related to the aggregation of emulsion

Ultrasonic power (w)	Particle size (nm)	ζ -potential (mV)	PDI	Emulsification yield (%)	Turbidity	TSI
200	594.2 ± 5.5 ^a	-26.90 ± 0.21 ^c	0.62 ± 0.01 ^a	75.01 ± 0.72 ^d	26,502.4 ± 250.1 ^a	4.91 ± 0.04 ^a
300	451.9 ± 4.0 ^b	-29.00 ± 0.24 ^c	0.36 ± 0.01 ^c	86.74 ± 0.84 ^c	24,732.7 ± 235.0 ^c	3.80 ± 0.03 ^c
400	295.6 ± 2.4 ^c	-33.40 ± 0.29 ^b	0.21 ± 0.01 ^d	90.03 ± 0.87 ^{ab}	24,659.0 ± 226.9 ^c	3.10 ± 0.02 ^d
500	291.8 ± 2.4 ^c	-34.30 ± 0.30 ^a	0.22 ± 0.01 ^d	91.04 ± 0.89 ^a	23,702.1 ± 227.0 ^d	3.01 ± 0.02 ^c
600	479.7 ± 4.3 ^b	-28.40 ± 0.23 ^d	0.51 ± 0.01 ^b	74.95 ± 0.71 ^d	25,018.1 ± 231.9 ^b	3.90 ± 0.03 ^b

Table 3. Effect of ultrasonic power on the characteristics and stability of nanoemulsions. Data represent mean ± standard deviations. Different letters in the same column represent a significant difference between samples ($p < 0.05$). Arrange all the averages in descending order, and use the letter “a” on the maximum average.

Ultrasonic time (min)	Particle size (nm)	ζ -potential (mV)	PDI	Emulsification yield (%)	Turbidity	TSI
6	589.7 ± 5.4 ^a	-26.40 ± 0.19 ^b	0.58 ± 0.01 ^a	76.13 ± 0.74 ^c	25,463.4 ± 247.3 ^a	4.90 ± 0.04 ^a
7	437.4 ± 4.0 ^b	-27.10 ± 0.21 ^b	0.40 ± 0.01 ^b	82.69 ± 0.80 ^b	24,856.2 ± 235.7 ^b	3.62 ± 0.03 ^b
8	295.6 ± 2.4 ^c	-33.40 ± 0.29 ^a	0.21 ± 0.00 ^c	90.03 ± 0.87 ^a	24,732.7 ± 234.4 ^b	3.13 ± 0.02 ^c
9	287.9 ± 2.4 ^c	-34.90 ± 0.31 ^a	0.18 ± 0.00 ^c	91.47 ± 0.90 ^a	24,614.1 ± 238.3 ^b	3.00 ± 0.02 ^c
10	468.5 ± 4.1 ^b	-27.60 ± 0.23 ^b	0.53 ± 0.01 ^a	76.24 ± 0.74 ^c	25,027.5 ± 243.1 ^a	3.81 ± 0.03 ^a

Table 4. Effect of ultrasonic power on the characteristics and stability of nanoemulsions. Data represent mean ± standard deviations. Different letters in the same column represent a significant difference between samples ($p < 0.05$). Arrange all the averages in descending order, and use the letter “a” on the maximum average.

molecules. The emulsification interface was unstable state under the condition of high ultrasonic power (600 W) output. At this time, the absolute value of the ζ -potential of the nanoemulsion was significantly reduced.

Effect of ultrasonication time. The effect of ultrasonic processing time on the properties of nanoemulsions is shown in Table 4. PDI, turbidity, and the particle size of the nanoemulsions decreased and the emulsification yield increased when the ultrasound time increased from 6 to 9 min. Properly increasing the ultrasonic time can improve the dispersion state and emulsion stability of nanoemulsion. When the ultrasound time was continuously increased (between 9 and 10 min), the particle size increased from 287.9 to 468.5 nm. The particle size of the nanoemulsions increased by longer sonication treatment. The effect of long-term sonication on particle size is related referred to in the literature as “over-processing”. Ultrasonication generated a large amount of energy, increasing the aggregation of droplets³⁴. Lago et al. observed a similar trend with ultrasonic treatment of emulsion particle size⁴². The greater turbulence and heating of the system increased the frequency of collisions between the oil balls and caused emulsion instability¹⁹. Over-processing also caused the ζ -potential value to decrease^{28,39,43}. Additionally, previous researchers found that long-term ultrasonication decreased the emulsion stability due to a decrease in interfacial tension and viscosity, while smaller interfacial tension values caused emulsion interface instability^{40,44}. Therefore, nanoemulsions exhibited satisfactory emulsion characteristics when the ultrasonic time was 9 min.

Ultrasonic nanoemulsion droplet structure. The 3D images help to observe the spatial structural morphology. In this study, the 3D confocal Raman imaging was used to observe the structure of SPI-PC nanoemulsion. The protein in emulsion exhibited significant Raman absorption at 1,660 cm^{-1} , and the feature regions were used for extraction and computational imaging. A microscopic image of a single drop in the yellow borderline region was analyzed in Fig. 1A. A Raman imaging structure of six nanoemulsion droplets (Fig. 1B) was formed as the observed position gradually probed into the center of the oil phase. The figure shows that a large number of green markers (SPI components) were more widely distributed in the oil–water interface of the emulsion droplets. It can be seen that soy protein were evenly distributed at the interface of nanoemulsion droplets according to our processing conditions.

Figure 2 shows the Raman characteristic absorption peak image of the emulsion. The symmetric stretching vibration and the anti-symmetric stretching vibration characteristic peak of the C–H₂ group of PC were 2,840 cm^{-1} and 2,880 cm^{-1} , respectively. The characteristic peak of amide I of SPI located at 1665 cm^{-1} . The results indicated that PC and SPI were distributed at the oil–water interface of the emulsion droplets, and our results were consistent with those of a previous study²⁰. The total Raman intensity decreased when the observed position gradually moved toward the center of the oil droplet, and this effect be related to the reduction of the soy protein content. However, the characteristic peaks of SPI and PC have not disappeared in the figure, which proved that SPI and PC were interacted and uniformly absorbed at the interface of the nanoemulsions.

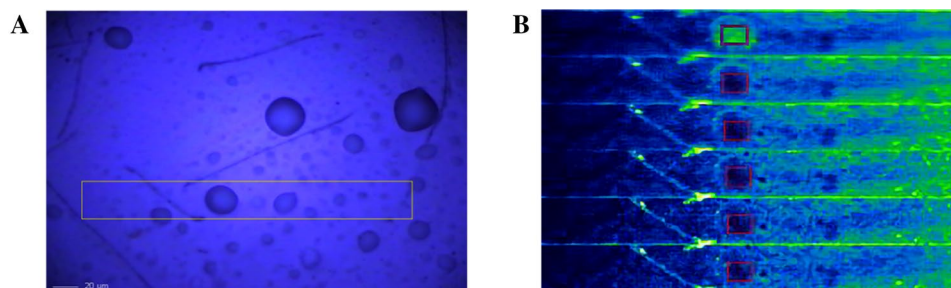


Figure 1. 3D-Raman microscopic image of ultrasonic preparation of nanoemulsions. In the figure, (A) a single nanoemulsions droplet was selected for analysis, and (B) 6 Raman imaging plots of the single nanoemulsions droplet were formed as the observational displacement gradually probed into the oil phase.

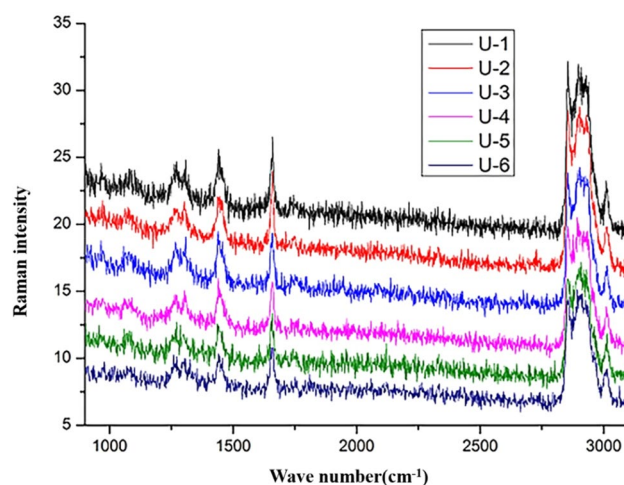


Figure 2. Raman image of the ultrasonic preparation of nanoemulsions. (U-1, U-2, U-3, U-4, U-5 and U-6 represent six observation positions from top to bottom, respectively).

The 3D images help to observe the spatial structural morphology. In this study, the 3D confocal Raman imaging was used to observe the structure of SPI-PC nanoemulsion. The protein in emulsion exhibited significant Raman absorption at $1,660\text{ cm}^{-1}$, and the feature regions were used for extraction and computational imaging. A microscopic image of a single drop in the yellow borderline region was analyzed in Fig. 1A. A Raman imaging structure of six nanoemulsion droplets (Fig. 1B) was formed as the observed position gradually probed into the center of the oil phase. The figure shows that a large number of green markers (SPI components) were more widely distributed in the oil–water interface of the emulsion droplets. It can be seen that soy protein were evenly distributed at the interface of nanoemulsion droplets according to our processing conditions.

Figure 2 shows the Raman characteristic absorption peak image of the emulsion. The symmetric stretching vibration and the anti-symmetric stretching vibration characteristic peak of the C-H₂ group of PC were $2,840\text{ cm}^{-1}$ and $2,880\text{ cm}^{-1}$, respectively. The characteristic peak of amide I of SPI located at $1,665\text{ cm}^{-1}$. The results indicated that PC and SPI were distributed at the oil–water interface of the emulsion droplets, and our results were consistent with those of a previous study²⁰. The total Raman intensity decreased when the observed position gradually moved toward the center of the oil droplet, and this effect be related to the reduction of the soy protein content. However, the characteristic peaks of SPI and PC have not disappeared in the figure, which proved that SPI and PC were interacted and uniformly absorbed at the interface of the nanoemulsions.

Storage stability of nanoemulsions. The stability of the product is essential for nanoemulsion-based delivery systems in most practical applications. Temperature, pH, storage time, processing method, and ionic strength can influence the stability of emulsions²⁰. Storage temperature and time are main factors influencing the stability of emulsions. The effects of different storage temperatures and storage times on nanoemulsion stability is shown in Table 5, When the storage temperature increased, the particle size increased, and the β -carotene retention and ζ -potential rate decreased with both storage temperature and time. The average particle size of the emulsion was maintained at 100–500 nm of nanodroplets, and the ζ -potential of the nanoemulsion was reduced to 35–30 mV during storage. The rate of liquid phase separation of nanoemulsions during storage also depends on the frequency of contact collisions between droplets, because Brownian motion increases as temperature storage increases. The droplet collision frequency affected the mass transfer kinetics of surfactant and oil mol-

Sample	Storage time (d)	4 °C	25 °C	55 °C
Particle size (nm)	0	288.1 ± 1.92 ^f	287.6 ± 1.51 ^f	288.2 ± 2.18 ^c
	5	290.4 ± 2.33 ^{de}	292.1 ± 3.21 ^f	338.2 ± 5.29 ^d
	10	292.3 ± 2.21 ^{cde}	302.1 ± 4.16 ^e	344.7 ± 2.15 ^{cd}
	15	294.4 ± 3.35 ^{cd}	319.5 ± 2.21 ^d	350.4 ± 4.14 ^c
	20	297.3 ± 2.38 ^{bc}	340.5 ± 5.19 ^c	361.2 ± 6.19 ^b
	25	300.2 ± 3.27 ^{ab}	353.3 ± 5.26 ^b	366.4 ± 3.15 ^{ab}
	30	304.4 ± 4.29 ^a	354.4 ± 5.28 ^a	372.1 ± 4.23 ^a
ζ-Potential (mV)	0	-33.3 ± 0.13 ^a	-33.2 ± 0.22 ^a	-33.3 ± 0.16 ^a
	5	-33.1 ± 0.12 ^{ab}	-32.8 ± 0.29 ^b	-32.9 ± 0.23 ^b
	10	-32.9 ± 0.19 ^b	-32.4 ± 0.21 ^c	-32.5 ± 0.26 ^c
	15	-32.6 ± 0.15 ^c	-31.7 ± 0.24 ^d	-31.7 ± 0.27 ^d
	20	-32.2 ± 0.21 ^d	-31.2 ± 0.18 ^c	-30.9 ± 0.17 ^c
	25	-31.9 ± 0.16 ^c	-30.7 ± 0.13 ^f	-30.3 ± 0.25 ^f
	30	-31.5 ± 0.17 ^f	-30.1 ± 0.24 ^g	-29.6 ± 0.23 ^g
β-Carotene retention rate (%)	0	98.5 ± 0.02 ^a	98.5 ± 0.01 ^a	98.5 ± 0.03 ^a
	5	94.2 ± 0.23 ^b	93.1 ± 0.31 ^b	92.4 ± 0.31 ^b
	10	92.6 ± 0.34 ^c	91.7 ± 0.46 ^c	90.2 ± 0.23 ^c
	15	91.2 ± 0.32 ^d	89.8 ± 0.51 ^d	88.7 ± 0.46 ^d
	20	89.3 ± 0.47 ^e	88.5 ± 0.38 ^e	87.5 ± 0.53 ^e
	25	88.1 ± 0.19 ^f	87.4 ± 0.27 ^f	86.4 ± 0.32 ^f
	30	87.8 ± 0.28 ^f	87.1 ± 0.26 ^f	86.1 ± 0.27 ^f

Table 5. Storage stability of nanoemulsion. Data represent mean ± standard deviations. Different letters in the same column represent a significant difference between samples ($p < 0.05$). Arrange all the averages in descending order, and use the letter “a” and “A” on the minimum average.

ecules between the water and oil phases, resulting in an increase of particle size⁴⁵. The ζ-potential value was an important indicator for the stability of the nanoemulsions. After storage at 4 °C, 25 °C, and 55 °C for 30 days, the absolute ζ-potential values of emulsions gradually decreased to 31.5, 30.1, and 29.6, respectively. This may be due to the aging of austenite and the change in protein conformation over time, leading to the formation of hydrophobic bonds and hydrogen bonds between adjacent proteins at the interface⁴⁶. Nanoemulsions had a lower electrostatic interaction while they were stored at high temperatures or during long-term storage, which caused the conformational change of the biopolymer of the surfactant molecules^{47–49}. The stability nanoemulsion is related to the storage environment (time, temperature). The nanoemulsions gradually oxidized during storage, and the degree of oxidation increased with the increase in storage time and temperature. Lipid oxidation might change the interfacial composition of the nanoemulsion, and cause the emulsifier to rearrange and desorb at the interface and reduce the stability of the emulsion system. Eventually, the nanoemulsions gradually broke up, which caused β-carotene to be released from the nanoemulsions.

Although the retention rate of β-carotene in the emulsion gradually decreased, 86% of β-carotene was remained even storing for a long time at a higher storage temperature (Table 5), exhibiting excellent resistance to droplet coalescence during storage. This may be due to the antioxidant activities of SPI and PC. Borba et al.⁵⁰ demonstrated that Tween 20 β-carotene nanoemulsions prepared by a high-pressure homogenizer had a retention rate of 70–80% during storage, and an increased ability to encapsulate β-carotene as compared to conventional emulsions. Early studies have found that protein emulsifiers inhibit lipid oxidation better than small-molecule surfactants^{51,52}. This provides a method to increase the potential use of carotenoids in the food industry, including applications of β-carotene.

Conclusions

In this research, the SPI-PC complex was used as the aqueous phase and sunflower oil was used as the oil phase, and the β-carotene nanoemulsion was prepared using ultrasonic technology. The results show that when SPI is 1.5%, PC is 0.22%, ultrasonic power is 500 W, ultrasonic time is 9 min, nanoemulsion has the best stability. 3D Raman imaging shows that ultrasonic treatment can make SPI and PC evenly distributed on the water–oil interface of nanoemulsion droplets. During storage, the ζ-potential and β-carotene retention rate were higher than 30 mV and 86%, respectively. The optimal preparation process provides a method and theoretical basis for the ultrasonic preparation of nanoemulsions, and may lead to further food design, including the design of β-carotene.

Received: 8 May 2020; Accepted: 23 July 2020

Published online: 19 August 2020

References

1. Aboalnaja, K. O., Yaghmoor, S., Kumosani, T. A. & McClements, D. J. Utilization of nanoemulsions to enhance bioactivity of pharmaceuticals, supplements, and nutraceuticals: nanoemulsion delivery systems and nanoemulsion excipient systems. *Expert Opin. Drug Deliv.* **13**, 1327 (2016).
2. Jin, H. *et al.* Fabrication of β -conglycinin-stabilized nanoemulsions via ultrasound process and influence of SDS and PEG 10000 co-emulsifiers on the physicochemical properties of nanoemulsions. *Food Res. Int.* **106**, 800–808 (2018).
3. Oca-Ávalos, *et al.* Nanoemulsions: stability and physical properties. *Curr. Opin. Food Sci.* **16**, 1–6 (2017).
4. O'Sullivan, J. J., Park, M., Beevers, J., Greenwood, R. W. & Norton, I. T. Applications of ultrasound for the functional modification of proteins and nanoemulsion formation: a review. *Food Hydrocoll.* **71**, S0268005X16311122 (2016).
5. Ghosh, V., Mukherjee, A. & Chandrasekaran, N. Ultrasonic emulsification of food-grade nanoemulsion formulation and evaluation of its bactericidal activity. *Ultrason. Sonochem.* **20**, 338–344 (2013).
6. Nazarzadeh, E., Anthonypillai, T. & Sajjadi, S. On the growth mechanisms of nanoemulsions. *J. Colloid Interface Sci.* **397**, 154–162 (2013).
7. Wang, S. *et al.* Influence of soy lecithin concentration on the physical properties of whey protein isolate-stabilized emulsion and microcapsule formation. *J. Food Eng.* **207**, 73–80 (2017).
8. Hoogevest, P. V. & Wendel, A. The use of natural and synthetic phospholipids as pharmaceutical excipients. *Eur. J. Lipid Sci. Technol.* **116**, 1088–1107 (2014).
9. Hirotsuka, M. *et al.* Increase in emulsification activity of soy lecithin-soy protein complex by ethanol and heat treatments. *J. Food Sci.* **49**, 1105–1110 (1984).
10. Shao, Y. & Tang, C.-H. Characteristics and oxidative stability of soy protein-stabilized oil-in-water emulsions: Influence of ionic strength and heat pretreatment. *Food Hydrocoll.* **37**, 149–158 (2014).
11. Li, Y. *et al.* Interaction of soybean protein isolate and phosphatidylcholine in nanoemulsions: A fluorescence analysis. *Food Hydrocoll.* **87**, 814–829. <https://doi.org/10.1016/j.foodhyd.2018.09.006> (2019).
12. Li, C. *et al.* Physicochemical properties of peanut protein isolate–glucmannan conjugates prepared by ultrasonic treatment. *Ultrason. Sonochem.* **21**, 1722–1727 (2014).
13. Song, H. Y., Moon, T. W. & Choi, S. J. Impact of antioxidant on the stability of beta-carotene in model beverage emulsions: Role of emulsion interfacial membrane. *Food Chem.* **279**, 194–201 (2019).
14. Li, J., Li, Y. & Guo, S. The binding mechanism of lecithin to soybean 11S and 7S globulins using fluorescence spectroscopy. *Food Sci. Biotechnol.* **23**, 1785–1791 (2014).
15. Kong, L., Bhosale, R. & Ziegler, G. R. Encapsulation and stabilization of β -carotene by amylose inclusion complexes. *Food Res. Int.* **105**, 446–452 (2017).
16. Thakkar, S. K., Bussie, M. D., Dixon, A. G. O. & Failla, M. L. Beta-carotene micellarization during in vitro digestion and uptake by Caco-2 cells is directly proportional to beta-carotene content in different genotypes of cassava. *J. Nutr.* **137**, 2229–2233 (2007).
17. Hou, Z. *et al.* Effect of chitosan molecular weight on the stability and rheological properties of β -carotene emulsions stabilized by soybean soluble polysaccharides. *Food Hydrocoll.* **26**, 205–211 (2012).
18. Sagalowicz, L. & Leser, M. E. Delivery systems for liquid food products. *Curr. Opin. Colloid Interface Sci.* **15**, 61–72 (2010).
19. Salvia-Trujillo, L., Rojas-Graü, A., Soliva-Fortuny, R. & Martín-Belloso, O. Physicochemical characterization and antimicrobial activity of food-grade emulsions and nanoemulsions incorporating essential oils. *Food Hydrocoll.* **43**, 547–556 (2015).
20. Li, Y. *et al.* Soy Protein isolate-phosphatidylcholine nanoemulsions prepared using high-pressure homogenization. *Nanomaterials* **8**, 307–318 (2018).
21. Li, D., Lu, L., Nan, X., Li, M. & Xie, X. Physical properties of oil-in-water nanoemulsions stabilized by OSA-modified starch for the encapsulation of lycopene. *Colloids Surf. A* **552**, 59–66 (2018).
22. Chen, W. *et al.* Impact of soy proteins, hydrolysates and monoglycerides at the oil/water interface in emulsions on interfacial properties and emulsion stability. *Colloids Surf. B Biointerfaces* **177**, 550–558 (2019).
23. Mao, L., Yang, J., Xu, D., Yuan, F. & Gao, Y. Effects of homogenization models and emulsifiers on the physicochemical properties of β -carotene nanoemulsions. *J. Dispers. Sci. Technol.* **31**, 986–993 (2010).
24. Cheong, A. M., Tan, C. P. & Nyam, K. L. Physicochemical, oxidative and anti-oxidant stabilities of kenaf seed oil-in-water nanoemulsions under different storage temperatures. *Ind. Crops Prod.* **95**, 374–382 (2017).
25. Hebshy, E., Buffa, M., Guamis, B., Blasco-Moreno, A. & Trujillo, A. J. Physical and oxidative stability of whey protein oil-in-water emulsions produced by conventional and ultra high-pressure homogenization: effects of pressure and protein concentration on emulsion characteristics. *Innov. Food Sci. Emerg. Technol.* **32**, 79–90 (2015).
26. Li, M., Ma, Y. & Cui, J. Whey-protein-stabilized nanoemulsions as a potential delivery system for water-insoluble curcumin. *LWT Food Sci. Technol.* **59**, 49–58 (2014).
27. Mehmood, T. *et al.* Optimization of olive oil based o/w nanoemulsions prepared through ultrasonic homogenization: a response surface methodology approach. *Food Chem.* **229**, 790–796 (2017).
28. Sui, X. *et al.* Impact of ultrasonic treatment on an emulsion system stabilized with soybean protein isolate and lecithin: its emulsifying property and emulsion stability. *Food Hydrocoll.* **63**, 727–734 (2017).
29. Berton-Carabin, C. C., Ropers, M. H. & Genot, C. Lipid oxidation in oil-in-water emulsions: involvement of the interfacial layer. *Compr. Rev. Food Sci. Food Saf.* **13**, 945–977 (2014).
30. Kim, H. *et al.* Formation of stable adhesive water-in-oil emulsions using a phospholipid and cosurfactants. *J. Ind. Eng. Chem.* **55**, 198–203 (2017).
31. Scuriatti, M. P., Tomás, M. C. & Wagner, J. R. Influence of soybean protein isolates-phosphatidylcholine interaction on the stability on oil-in-water emulsions. *J. Am. Oil Chem. Soc.* **80**, 1093–1100 (2003).
32. Nieuwenhuysen, W. V. & Szuhaj, B. F. Effects of lecithins and proteins on the stability of emulsions. *Eur. J. Lipid Sci. Technol.* **100**, 282–291 (1998).
33. Maldonado-Valderrama, J. & Patino, J. M. R. Interfacial rheology of protein–surfactant mixtures. *Curr. Opin. Colloid Interface Sci.* **15**, 271–282 (2010).
34. Floury, J., Desrumaux, A. & Lardieres, J. Effect of high-pressure homogenization on droplet size distributions and rheological properties of model oil-in-water emulsions. *Innov. Food Sci. Emerg. Technol.* **1**, 127–134 (2000).
35. Dickinson, E. & Golding, M. Rheology of sodium caseinate stabilized oil-in-water emulsions. *J. Colloid Interface Sci.* **191**, 166–176 (1997).
36. Martínez, K. D. *et al.* Effect of dynamic high-pressure treatment on the interfacial and foaming properties of soy protein isolate–hydroxypropylmethylcelluloses systems. *Food Hydrocoll.* **25**, 1640–1645 (2011).
37. Wang, B. *et al.* Effect of concentrated flaxseed protein on the stability and rheological properties of soybean oil-in-water emulsions. *J. Food Eng.* **96**, 555–561 (2010).
38. Tang, S. Y. *et al.* Formulation development and optimization of a novel cremophore el-based nanoemulsion using ultrasound cavitation. *Ultrason. Sonochem.* **19**, 330–345 (2012).
39. Kentish, S. *et al.* The use of ultrasonics for nanoemulsion preparation. *Innov. Food Sci. Emerg. Technol.* **9**, 170–175 (2008).
40. Kishore, R. S. K. *et al.* Degradation of polysorbates 20 and 80: studies on thermal autoxidation and hydrolysis. *J. Pharm. Sci.* **100**, 721–731 (2011).

41. Shanmugam, A. & Ashokkumar, M. Ultrasonic preparation of stable flax seed oil emulsions in dairy systems: physicochemical characterization. *Food Hydrocoll.* **39**, 151–162 (2014).
42. Lago, A. M. T. *et al.* Ultrasound-assisted oil-in-water nanoemulsion produced from *Pereskia aculeata* miller mucilage. *Ultrason. Sonochem.* **50**, 339–353 (2019).
43. Heesoo, P., Saehun, M. & Yong-Ro, K. UV and storage stability of retinol contained in oil-in-water nanoemulsions. *Food Chem.* **272**, 404–410 (2019).
44. Akbas, E., Soyler, B. & Oztop, M. H. Formation of capsaicin loaded nanoemulsions with high pressure homogenization and ultrasonication. *LWT Food Sci. Technol.* **96**, 266–273 (2018).
45. Carpenter, J. & Saharan, V. K. Ultrasonic assisted formation and stability of mustard oil in water nanoemulsion: effect of process parameters and their optimization. *Ultrason. Sonochem.* **35**, 422–430 (2017).
46. Tcholakova, S., Denkov, N. D., Ivanov, I. B. & Campbell, B. Coalescence stability of emulsions containing globular milk proteins. *Adv. Coll. Interface. Sci.* **123–126**, 259–293 (2006).
47. Cortés-Muñoz, M., Chevalier-Lucia, D. & Dumay, E. Characteristics of submicron emulsions prepared by ultra-high pressure homogenisation: Effect of chilled or frozen storage. *Food Hydrocoll.* **23**, 640–654 (2009).
48. Li, P. H. & Lu, W. C. Effects of storage conditions on the physical stability of D-limonene nanoemulsion. *Food Hydrocoll.* **53**, 218–224 (2016).
49. Abbas, S. *et al.* An overview of ultrasound-assisted food-grade nanoemulsions. *Food Eng. Rev.* **5**, 139–157 (2013).
50. Borba, C. M. *et al.* Physical and chemical stability of β -carotene nanoemulsions during storage and thermal process. *Food Res. Int.* **121**, 229–237 (2019).
51. Tan, C. P. & Nakajima, M. Effect of polyglycerol esters of fatty acids on physicochemical properties and stability of β -carotene nanodispersions prepared by emulsification/evaporation method. *J. Sci. Food Agric.* **85**, 121–126 (2005).
52. Haahr, A.-M. & Jacobsen, C. Emulsifier type, metal chelation and pH affect oxidative stability of n-3-enriched emulsions. *Eur. J. Lipid Sci. Technol.* **110**, 949–961 (2008).

Acknowledgements

This research was funded by University Nursing program for Young Scholars with Creative Talents in Heilongjiang Province (UNPYSCT-2017015); Major Projects in Research and Development of Applied Technology in Heilongjiang (GY2017ZB0017); Heilongjiang Provincial Science Foundation Project (C2018024); China Postdoctoral Science Foundation (2018M641798); Heilongjiang Provincial Postdoctoral Science Foundation (LBH-Z18030). The authors appreciate Yves Harimana and Denise R. for language review.

Author contributions

Y.L. and Z.W. conceived and designed the experiments; F.T., M.H., J.X. and F.C. performed the experiments; F.T., M.H. and C.W. analyzed the data; F.T. and M.H. wrote—original draft preparation; all authors wrote—review and edit; all authors have read and agreed to the published version of the manuscript.

Competing interests


The authors declare no competing interests.

Additional information

Correspondence and requests for materials should be addressed to Y.L.

Reprints and permissions information is available at www.nature.com/reprints.

Publisher's note Springer Nature remains neutral with regard to jurisdictional claims in published maps and institutional affiliations.

 **Open Access** This article is licensed under a Creative Commons Attribution 4.0 International License, which permits use, sharing, adaptation, distribution and reproduction in any medium or format, as long as you give appropriate credit to the original author(s) and the source, provide a link to the Creative Commons license, and indicate if changes were made. The images or other third party material in this article are included in the article's Creative Commons license, unless indicated otherwise in a credit line to the material. If material is not included in the article's Creative Commons license and your intended use is not permitted by statutory regulation or exceeds the permitted use, you will need to obtain permission directly from the copyright holder. To view a copy of this license, visit <http://creativecommons.org/licenses/by/4.0/>.

© The Author(s) 2020